

Collective Coordinate Control of Density Distributions

Obioma U. Uche,¹ Salvatore Torquato,^{2,3} and Frank H. Stillinger²

¹*Department of Chemical Engineering,
Princeton University, Princeton, NJ 08544*

²*Department of Chemistry, Princeton University, Princeton, NJ 08544*

³*Princeton Institute for the Science and Technology of Materials,
Princeton University, Princeton, NJ 08544*

(Dated: February 6, 2008)

Abstract

Real collective density variables $C(\mathbf{k})$ [c.f. Eq.1.3)] in many-particle systems arise from non-linear transformations of particle positions, and determine the structure factor $S(\mathbf{k})$, where \mathbf{k} denotes the wave vector. Our objective is to prescribe $C(\mathbf{k})$ and then to find many-particle configurations that correspond to such a target $C(\mathbf{k})$ using a numerical optimization technique. Numerical results reported here extend earlier one- and two-dimensional studies to include three dimensions. In addition, they demonstrate the capacity to control $S(\mathbf{k})$ in the neighborhood of $|\mathbf{k}| = 0$. The optimization method employed generates multi-particle configurations for which $S(\mathbf{k}) \propto |\mathbf{k}|^\alpha$, $|\mathbf{k}| \leq K$, and $\alpha = 1, 2, 4, 6, 8$, and 10 . The case $\alpha = 1$ is relevant for the Harrison-Zeldovich model of the early universe, for superfluid ^4He , and for jammed amorphous sphere packings. The analysis also provides specific examples of interaction potentials whose classical ground state are configurationally degenerate and disordered.

1. INTRODUCTION

Spatial arrangements of particles in many-body systems exhibit wide diversity that arises from the interactions that are present, and from the prior history of those systems. One of the available analytical tools that has proved useful for describing those spatial arrangements, whether for individual cases or for ensemble averages, is the set of collective density variables. These are conventionally defined for N identical particles in the following way:

$$\rho(\mathbf{k}) = \sum_{j=1}^N \exp(i\mathbf{k} \cdot \mathbf{r}_j) \quad (1.1)$$

where \mathbf{r}_j denotes the location of particle j , and the \mathbf{k} are the wave vectors appropriate for the containing volume and boundary conditions.

Collective density variables have played an important role in a variety of problems in condensed matter physics. Specifically, they have been used in illustrating that large-scale density variations in superfluid ${}^4\text{He}$ are in fact long-wavelength phonons [1]. Introduction of the appropriate collective coordinates is natural in describing independent plasma oscillations brought about by the long-range Coulomb interactions between electrons in metals [2]. Furthermore, application of these variables has aided in the derivation of self-consistent integral equations for pair correlation functions in classical fluids [3], in obtaining corrections to the random phase approximation for the electron gas [4], and in generating classical ground states for particle systems [5–7]. But in spite of the fact that collective density variables appear widely in the literature [1–10], the nonlinearity of the transformation in Eq. (1.1) from particle positions to collective variables entails nontrivial mathematical properties that are still incompletely understood [5, 6]. The present paper is devoted to clarifying some of the remaining issues.

Many physical applications of collective density variables focus on the structure factor $S(\mathbf{k})$ for the many-particle system involved:

$$\begin{aligned} S(\mathbf{k}) &= \frac{|\rho(\mathbf{k})|^2}{N} \\ &= 1 + \frac{2}{N} C(\mathbf{k}) \end{aligned} \quad (1.2)$$

where the real quantities $C(\mathbf{k})$ are the following:

$$C(\mathbf{k}) = \sum_{j=1}^{N-1} \sum_{l=j+1}^N \cos[\mathbf{k} \cdot (\mathbf{r}_j - \mathbf{r}_l)]. \quad (1.3)$$

In view of the fact that the phase angles of the $\rho(\mathbf{k})$ are irrelevant for most applications, it suffices to focus attention on the $C(\mathbf{k})$'s.

A considerable challenge involves determining what sets of $C(\mathbf{k})$ values correspond to attainable particle configurations, and how to generate and describe those special configurations, including ground-state structures. In particular, it is important to understand the extent to which these real collective variables at small wave vectors \mathbf{k} are controllable. Although we begin by considering the general situation, much of the attention in the following will involve the examination of “hyperuniform” systems [11, 12], namely those in the infinite system limit for which:

$$\lim_{\mathbf{k} \rightarrow 0} S(\mathbf{k}) = 0. \quad (1.4)$$

This defining characteristic of hyperuniformity states that the usual mean-square particle-number fluctuations increases less than R^d , where R denotes the linear size of an observation window and d is the space dimension [11]. Considering the fact that various hyperuniform physical systems exhibit characteristic \mathbf{k} dependence of their structure factors near the origin (*e.g.*, the ground state of liquid ${}^4\text{He}$ [13–15] as well as random, jammed hard-sphere packings [16] and the early Universe [17]), it becomes important to understand what N -particle configurational implications stem from these specific $S(\mathbf{k})$ forms. This has guided the analysis detailed below.

Because our objective is to prescribe $C(\mathbf{k})$ [or, equivalently $S(\mathbf{k})$] and then to find many-particle configurations that may correspond to such a target structure function, this problem can be regarded to be an *inverse problem*. The analogous inverse problem in real space in which the pair correlation function is prescribed has received considerable attention in the last several years [18–22]. This class of inverse problems has come to be called *construction* problems [18–21]. *A priori*, a prescribed pair structural function is not necessarily realizable by a many-particle configuration. A solution to the construction problem therefore provides numerical evidence for realizability of a target pair structural function. Thus, the present investigation has important implications for the *realizability* problem of statistical mechanics, which seeks to determine the necessary conditions that a prescribed pair correlation [or its

equivalent Fourier representation, $S(\mathbf{k})]$ must possess in order for it to correspond to a many-particle system [19, 22, 23].

The present paper extends our earlier one-dimensional [5] and two-dimensional [6] studies of collective coordinate control of density distributions. Our focus in these two studies was to consider continuous and bounded pair potentials and to constrain the corresponding collective parameters $C(\mathbf{k})$, with wave vector \mathbf{k} magnitudes at or below a chosen cutoff, to their absolute minimum values. In other words, density fluctuations for those \mathbf{k} 's were completely suppressed. In our two-dimensional investigation [6], we were able to distinguish between three different ground-state structural regimes as the number of constrained wave vectors were increased - disordered, wavy crystalline, and crystalline regimes. Evidence for a disordered or irregular ground state, a counterintuitive notion, had heretofore not been provided. In the present work, we extend these results not only to three-dimensional ground state problems but to more general two- and three-dimensional hyperuniform many-particle systems.

The next section provides some of the mathematical structure needed to understand how fixing values of sets of the real collective variables $C(\mathbf{k})$ exerts control over the allowed many-particle configurations. A description of our numerical methods for analyzing this problem follows in Section 3. Results of the numerical study cover both two- and three-dimensional systems, and are presented respectively in Sections 4 and 5. Among other results, we provide specific examples of interaction potentials whose classical ground state are configurationally degenerate and disordered. Our conclusions and discussion of some remaining issues appear in Section 6.

2. GENERAL RELATIONS

Suppose that the N point particles reside in a one-, two-, or three-dimensional container that is an L_x interval, an $L_x \times L_y$ rectangle, or an $L_x \times L_y \times L_z$ rectangular solid. Furthermore, suppose that periodic boundary conditions apply. The applicable wave vectors have components:

$$k_\gamma = \frac{2\pi n_\gamma}{L_\gamma} \quad (n_\gamma = 0, \pm 1, \pm 2, \dots) \quad (2.1)$$

where $\gamma = x, y, z$ as needed. It is easy to see that the $C(\mathbf{k})$ must obey the following properties:

$$\begin{aligned} C(0) &= \frac{1}{2}N(N-1) , \\ C(\mathbf{k}) &= C(-\mathbf{k}) . \end{aligned} \tag{2.2}$$

Furthermore, these collective variables are necessarily confined to the range:

$$-\frac{1}{2}N \leq C(\mathbf{k}) \leq \frac{1}{2}N(N-1) \quad (\mathbf{k} \neq 0) , \tag{2.3}$$

and as they vary over this range they measure the magnitude of density inhomogeneity at wave vector \mathbf{k} in the N -particle system.

Although the number of collective variables is infinite, the N -particle system possesses only dN configurational degrees of freedom, where d is the Euclidean space dimension ($d = 1, 2, 3$). Consequently, it is unreasonable to suppose (barring special circumstances) that generally all $C(\mathbf{k})$'s could be independently controlled. However it is possible, as examples in Refs. [5, 6] and in subsequent sections below will illustrate, to specify simultaneously a number of the collective variables equal to a significant fraction of dN . In particular, let \mathbf{Q} be a finite set of the \mathbf{k} 's meeting this criterion, and let $C_0(\mathbf{k})$ be the target value to which $C(\mathbf{k})$ is to be constrained. Of course, each $C_0(\mathbf{k})$ must lie in the range specified by inequalities (2.3) above. Then consider the following non-negative objective function:

$$\begin{aligned} \Phi(\mathbf{r}_1 \dots \mathbf{r}_N) &= \sum_{\mathbf{k} \in \mathbf{Q}} V(\mathbf{k})[C(\mathbf{k}) - C_0(\mathbf{k})]^2 , \\ V(\mathbf{k}) &= V(-\mathbf{k}) > 0 . \end{aligned} \tag{2.4}$$

This continuous and differentiable function of the particle coordinates attains its absolute minimum value zero if and only if the $C(\mathbf{k})$ for all $\mathbf{k} \in \mathbf{Q}$ equal their target values.

By inserting the definitions (1.3) for the collective variables into Eq. (2.4), one trivially has the following

$$\Phi(\mathbf{r}_1 \dots \mathbf{r}_N) = \sum_{\mathbf{k} \in \mathbf{Q}} V(\mathbf{k}) \left\{ \sum_{j < l}^N \sum_{m < n}^N \cos[\mathbf{k} \cdot (\mathbf{r}_j - \mathbf{r}_l)] \cos[\mathbf{k} \cdot (\mathbf{r}_m - \mathbf{r}_n)] - 2C_0(\mathbf{k}) \sum_{j < l}^N \cos[\mathbf{k} \cdot (\mathbf{r}_j - \mathbf{r}_l)] + C_0^2(\mathbf{k}) \right\} . \tag{2.5}$$

The right member of this last equation can be resolved into symmetric combinations of four, three, and two particle contributions, plus an additive constant:

$$\Phi(\mathbf{r}_1 \dots \mathbf{r}_N) = \sum_{j < l < m < n}^N v_4(\mathbf{r}_j, \mathbf{r}_l, \mathbf{r}_m, \mathbf{r}_n) + \sum_{j < l < m}^N v_3(\mathbf{r}_j, \mathbf{r}_l, \mathbf{r}_m) + \sum_{j < l}^N v_2(\mathbf{r}_j, \mathbf{r}_l) + \Phi_0 . \quad (2.6)$$

The specific forms of these contributions are as follows:

$$\begin{aligned} v_4(\mathbf{r}_j, \mathbf{r}_l, \mathbf{r}_m, \mathbf{r}_n) &= 2 \sum_{\mathbf{k} \in \mathbf{Q}} V(\mathbf{k}) \{ \cos[\mathbf{k} \cdot (\mathbf{r}_j - \mathbf{r}_l)] \cos[\mathbf{k} \cdot (\mathbf{r}_m - \mathbf{r}_n)] \\ &\quad + \cos[\mathbf{k} \cdot (\mathbf{r}_j - \mathbf{r}_m)] \cos[\mathbf{k} \cdot (\mathbf{r}_l - \mathbf{r}_n)] + \cos[\mathbf{k} \cdot (\mathbf{r}_j - \mathbf{r}_n)] \cos[\mathbf{k} \cdot (\mathbf{r}_l - \mathbf{r}_m)] \} , \\ v_3(\mathbf{r}_j, \mathbf{r}_l, \mathbf{r}_m) &= 2 \sum_{\mathbf{k} \in \mathbf{Q}} V(\mathbf{k}) \{ \cos[\mathbf{k} \cdot (\mathbf{r}_j - \mathbf{r}_l)] \cos[\mathbf{k} \cdot (\mathbf{r}_j - \mathbf{r}_m)] \\ &\quad + \cos[\mathbf{k} \cdot (\mathbf{r}_l - \mathbf{r}_j)] \cos[\mathbf{k} \cdot (\mathbf{r}_l - \mathbf{r}_m)] + \cos[\mathbf{k} \cdot (\mathbf{r}_m - \mathbf{r}_j)] \cos[\mathbf{k} \cdot (\mathbf{r}_m - \mathbf{r}_l)] \} , \\ v_2(\mathbf{r}_j, \mathbf{r}_l) &= \sum_{\mathbf{k} \in \mathbf{Q}} V(\mathbf{k}) \{ \cos^2[\mathbf{k} \cdot (\mathbf{r}_j - \mathbf{r}_l)] - 2C_0 \cos[\mathbf{k} \cdot (\mathbf{r}_j - \mathbf{r}_l)] \} , \\ \Phi_0 &= \sum_{\mathbf{k} \in \mathbf{Q}} V(\mathbf{k}) C_0^2(\mathbf{k}) . \end{aligned} \quad (2.7)$$

If Φ is interpreted as a potential energy of interaction for the N point particles, then Eqs. (2.6) and (2.7) specify four, three, and two particle interaction potentials operating in the system. If classical ground-state configurations for the N particles subject to that potential exist for which $\Phi = 0$, then those configurations necessarily attain the desired target values of the collective variables.

The remainder of our analysis will be restricted to cases for which the wave vector set \mathbf{Q} consists of all those \mathbf{k} lying within a given distance from the origin:

$$\mathbf{Q} : 0 \leq |\mathbf{k}| \leq K . \quad (2.8)$$

In addition, we shall also confine attention to the following specific family of forms for $C_0(\mathbf{k})$:

$$C_0(\mathbf{k}) = -N/2 + D|\mathbf{k}|^\alpha , \quad (2.9)$$

where the multiplicative constant D and the exponent α are both non-negative. This choice focuses on the behavior of the particle system in the hyperuniform regime.

Previous work [5, 6] only considered the situation where $D = 0$, *i.e.*, each of the constrained collective variables was required to be at its minimum value $-N/2$. In that event,

it is possible to utilize a simpler potential energy (objective) function $\tilde{\Phi}$ that reduces to a sum of just two-particle interactions:

$$\tilde{\Phi}(\mathbf{r}_1 \dots \mathbf{r}_N) = \Omega^{-1} \sum_{\mathbf{k} \in \mathbf{Q}} \tilde{V}(\mathbf{k}) C(\mathbf{k}) , \quad (2.10)$$

In this expression Ω is the system length (L_x), area ($L_x L_y$), or volume ($L_x L_y L_z$), and

$$\tilde{V}(\mathbf{k}) = \tilde{V}(-\mathbf{k}) > 0 . \quad (2.11)$$

It is easy to show [5, 6] that Eq. (2.10) is equivalent to:

$$\begin{aligned} \tilde{\Phi}(\mathbf{r}_1 \dots \mathbf{r}_N) &= \sum_{j < l}^N \tilde{v}_2(\mathbf{r}_j, \mathbf{r}_l) , \\ \tilde{v}_2(\mathbf{r}_j, \mathbf{r}_l) &= \Omega^{-1} \sum_{\mathbf{k} \in \mathbf{Q}} \tilde{V}(\mathbf{k}) \exp[i\mathbf{k} \cdot (\mathbf{r}_j - \mathbf{r}_l)] . \end{aligned} \quad (2.12)$$

On account of the positivity condition (2.11) on $\tilde{V}(\mathbf{k})$, the absolute minimum of $\tilde{\Phi}$ will have the value:

$$\min_{\mathbf{r}_1 \dots \mathbf{r}_N} (\tilde{\Phi}) = -N/2 \sum_{\mathbf{k} \in \mathbf{Q}} \tilde{V}(\mathbf{k}) \quad (2.13)$$

if and only if there exist particle configurations satisfying all of the collective variable constraints. Of course the more elaborate (and more general) formulation defined by Eqs. (2.4)-(2.7) is also applicable to this $D = 0$ case.

Suppose that system configurations have been found which succeed in producing the desired target values for collective variables over the wave vector set \mathbf{Q} . Then these configurations obviously satisfy the same target values over the smaller wave vector set $\mathbf{Q}' \subset \mathbf{Q}$. But in view of the fact that \mathbf{Q}' entails fewer configurational constraints, one can expect that a more inclusive set of N -particle configurations satisfies those constraints. Indeed that is exactly what has been found in our previous one- and two-dimensional studies [5, 6], and further two- and three-dimensional examples will be reported in this paper. With respect to the objective functions Φ and $\tilde{\Phi}$ whose minimization indicates a solution to the constraint problem, the corresponding potential energy interpretations demonstrate the presence of configurationally *degenerate* classical ground states for the N particles, including disordered or highly irregular ground-state structures. This ground-state degeneracy phenomenon has

been the subject of a recent theoretical study [7] that proceeds in a rather different direction than from the collective coordinate perspective presented here. The key idea used by Sütő to prove a theorem about ground states is that the Fourier transform of the pair potential $V(k)$ be nonnegative with compact support, which was first employed in Ref. [5]; see also Ref. [6].

3. COMPUTATIONAL METHODS

In all calculations reported below, we assume that the system region Ω is constrained to a unit square in two dimensions or a unit cube in three dimensions, to which periodic boundary conditions are applied. Special attention is devoted to the choice of the system population N for both two and three dimensions. In two dimensions, N has been chosen such that all particles could be arranged in the square simulation box in an aligned and nearly undeformed version of the triangular lattice. For this purpose, the system occupancy N is required to be the product of integers $2pq$ where the rational number p/q is a close approximation to the irrational number $3^{1/2}$. The corresponding configuration consists of $2q$ rows of p particles. The same approach was used in selecting the system size in our earlier two-dimensional study [6]. In three dimensions, N is selected such that all particles can be assembled as an aligned face-centered cubic lattice. Thus, the system occupancy is $N = 4s^3$ particles where s is a non-zero integer.

For any given choice of the independent parameters N , K , D , and α , the majority of our numerical studies utilized a random number generator to create an initial configuration of the particles inside the simulation space Ω . As one would expect, this starting point typically produces a large positive value of the objective function of interest. We consider the specific case of Eq. (2.4) where $V(k)$ is unity for the set Q under consideration. Introduction of the original configuration to the numerical optimization tool MINOP [24, 25] results in a search for a particle pattern at the absolute minimum of the objective function. Our earlier two-dimensional study [6] involved use of the conjugate gradient method [27] as our numerical tool of choice. The greater utility of the MINOP optimization technique for the present investigation has been an important advantage that merits brief discussion.

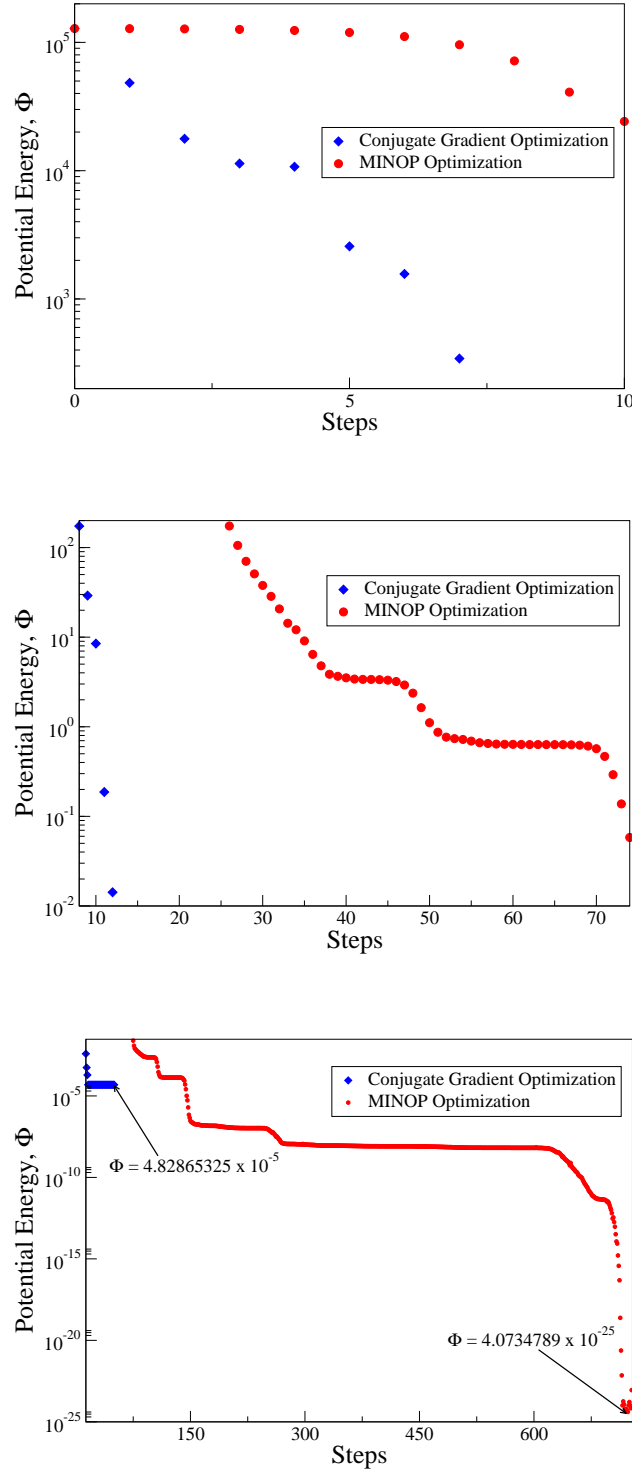


FIG. 1: (Color online) Tracking of the potential energy for conjugate gradient and MINOP algorithms. Top panel: Early steps. Middle panel: Intermediate steps. Bottom panel: Late Steps. It should be noted that both algorithms were applied to the same $d = 1$ minimization problem and initial particle configuration. The relevant parameters for the minimization problem are $N = 200$, $K = 10\pi$, $\alpha = 6$, and $DK^6 = 0.01$.

The three plots in Fig. 1 display the tracked potential energy Φ during the course of a minimization for both conjugate gradient (CG) and MINOP optimizations. Here, we have applied the algorithms to Φ minimization for a one-dimensional system with the parameters $N = 200$, $K = 10\pi$, $\alpha = 6$, and $DK^6 = 0.01$. The final values of the objective function Φ are typical for several cases examined and clearly indicate that the MINOP strategy is better suited to finding a numerically precise solution to the problem than is the conjugate gradient approach. This significant disparity can be attributed to details of the multidimensional Φ “landscape” and to the innate differences between the two algorithms. In CG optimization, minimization proceeds in a direction conjugate to the old gradient, *i.e.*, that the change in the function gradient be perpendicular to the most recent previous direction of minimization. In contrast, the MINOP [24] (“dogleg”) strategy is as follows:

Step 0 Let Δ_i be a pre-set step bound, \mathbf{p}_i be the Cauchy step, and \mathbf{n}_i be the Newton step,
i.e.,

$$\mathbf{p}_i = (|\mathbf{g}_i|^2 / \mathbf{g}_i^T \mathbf{G}_i \mathbf{g}_i) \mathbf{g}_i \quad \mathbf{n}_i = -\mathbf{H}_i \mathbf{g}_i$$

where \mathbf{g}_i , \mathbf{G}_i , and \mathbf{H}_i are the gradient, the Hessian approximation, and its inverse at the i th iteration respectively.

Step 1 Compute \mathbf{n}_i and $|\mathbf{n}_i|$. If $|\mathbf{n}_i| \leq \Delta_i$, we take $\Delta \mathbf{x}_i = \mathbf{n}_i$. If $|\mathbf{n}_i| > \Delta_i$, we compute $|t\mathbf{n}_i|$, where t is defined in Ref. [24]. If $|t\mathbf{n}_i| \leq \Delta_i$, we take $\mathbf{x}_i = (\Delta_i / |\mathbf{n}_i|) \mathbf{n}_i$.

Step 2 If $|t\mathbf{n}_i| > \Delta_i$, we then compute the Cauchy step; and, if $|\mathbf{p}_i| \geq \Delta_i$, we take $\Delta \mathbf{x}_i = -(\Delta_i / |\mathbf{g}_i|) \mathbf{g}_i$.

Step 3 If $|\mathbf{p}_i| < \Delta_i$, we take $\Delta \mathbf{x}_i = (1 - \theta_i) \mathbf{p}_i + \theta_i t \mathbf{n}_i$, where θ_i is chosen such that $0 < \theta_i < 1$ and $|\Delta \mathbf{x}_i| = \Delta_i$.

The MINOP algorithm minimizes a real-valued function of any number of variables based on user-provided first derivative and function information. In general, it applies a dogleg strategy which uses a gradient direction when one is far, a quasi-Newton direction when one is close, and a linear combination of the two when at intermediate distances from a solution.

4. RESULTS - TWO DIMENSIONS

We have performed numerical simulations on a variety of system sizes, random initial configurations, numbers of constrained vectors (*i.e.*, K cutoff), and choices for the independent parameters D and α . Calculations have proceeded to attain high precision for the absolute minimum of the objective function of interest, Φ or $\tilde{\Phi}$. Note that some initial configurations have not yielded the global minimum of the objective function hypersurface. In such cases, it can be inferred that there exist some relative minima along the objective function’s hypersurface landscape. However, all cases that are reported below in our analysis involve the absolute minimum of the objective function.

In order to simplify the presentation of our results, we introduce the following parameter

$$\chi = \frac{M(K)}{dN} \quad (4.1)$$

where $M(K)$ is defined as the number of independently constrained collective coordinates and d indicates the system dimension. The parameter χ is the ratio of the number of constrained degrees of freedom to the total number of degrees of freedom in the investigated system and has proved to be a fundamental descriptor in the prior one- and two-dimensional studies [5, 6].

In the following two subsections, we present the results produced by application of the MINOP algorithm to minimization of the objective function Φ for two-dimensional particle systems. In the first subsection, we demonstrate the ability to tailor the small- $|\mathbf{k}|$ portion of the structure factor associated with point particle systems. In the latter subsection, we study the effect of manipulating the structure factor $S(k)$ within the distinctive “wavy crystalline” regime reported previously in Ref. [6].

4.1. Tailoring the Structure Factor - Two Dimensions

This section describes our successful attempts to manipulate the structure factor $S(k)$ of two-dimensional point particle systems. We subjected the objective function Φ with a randomly generated initial configuration to the MINOP algorithm in order to evolve the

$C(\mathbf{k})$'s toward their target values. Our numerical simulations have involved the use of 168- and 418-particle systems. Note that these system sizes are the same as those studied in Ref. [6]. In addition, we vary the \mathbf{k} -space range parameter K ($2\pi \leq K \leq 40\pi$) and the multiplicative parameter D ($0.01 \leq DK^\alpha \leq 150$). We have varied α , a key parameter determining the nature of the tailored structure factor. In particular, we have generated solutions for the Harrison-Zeldovich [17] spectrum ($\alpha = 1$) as well as for the $\alpha = 4, 6, 8$, and 10 minimization problems. We devoted much of our study to the $\alpha = 1$ and 6 minimization problems with less detailed attention to the $\alpha = 4, 8$, and 10 minimization cases. As discussed below, our results demonstrate wide latitude in the capacity to control the structure factor for two-dimensional point particle systems.

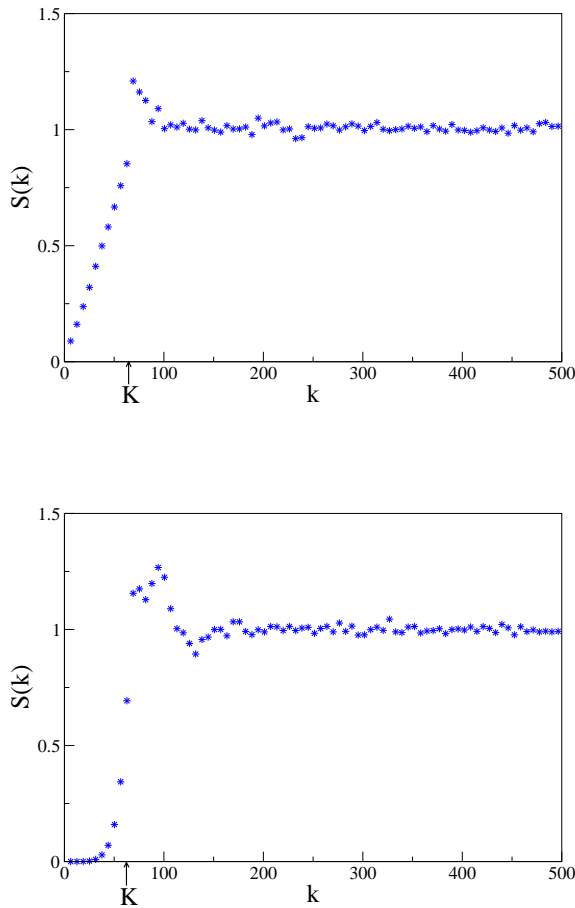


FIG. 2: (Color online) Averaged structure factor plots for the two-dimensional minimization problem. The relevant parameters are $N = 168$, $K = 20\pi$, $DK^\alpha = 75$, $\chi = 0.470238$. Top panel: Harrison-Zeldovich linear spectrum for small k . Bottom panel: $|\mathbf{k}|^6$ spectrum. Each structure factor is averaged over 50 realizations.

Plots of the system structure factor that have been tailored to fit the linear Harrison-Zeldovich and $|\mathbf{k}|^6$ spectra are shown in Fig. 2. Here, the structure factor is derived from final configurations via Eq. 1.2 and averaged over 50 independent realizations. For the purposes of graphical representation, the structure factor is binned over the reported range of \mathbf{k} -space. Note that by construction, the contributions to $S(k)$ below the cutoff K for a specific set of parameters (fixed N , K , D , and α) are identical for each realization. Outside the cutoff, the $S(k)$ contributions from each realization deviate irregularly from one another,

but their average for $|\mathbf{k}| > K$ shows a weak maximum followed by quick decay to unity as $|\mathbf{k}|$ increases. From these structure factor plots, it is evidently possible to tailor the structure factor to either spectrum. In particular, the respective linear and sextic nature of the plots at low k are visually clear.

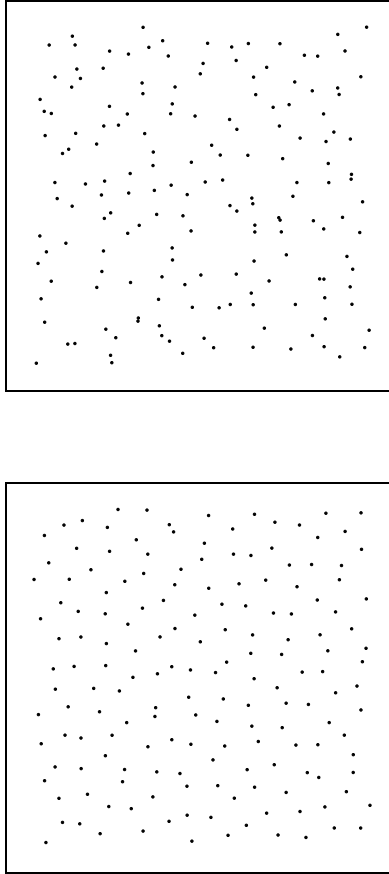


FIG. 3: Typical two-dimensional final configurations for the investigated spectra. The relevant parameters are $N = 168$, $K = 20\pi$, $DK^\alpha = 75$, $\chi = 0.470238$. Top panel: Harrison-Zeldovich linear spectrum. Bottom panel: $|\mathbf{k}|^6$ spectrum.

Figure 3 displays sample two-dimensional final configurations generated by the Φ minimization problem for the linear Harrison-Zeldovich and $|\mathbf{k}|^6$ spectra. The lack of any visible long-range regularity is apparent in the pictured configurations for both cases. However, some random point clustering appears to be present in the accompanying configuration for the Harrison-Zeldovich spectrum. This differs from the $|\mathbf{k}|^6$ spectrum configuration in which an effective repelling particle core appears to be present. Finally, we mention that corresponding analysis of the $|\mathbf{k}|^4$, $|\mathbf{k}|^8$, and $|\mathbf{k}|^{10}$ spectra minimization problems yield results

consistent with the above observations, providing systematic pattern sequences in both \mathbf{r} and \mathbf{k} spaces as illustrated in Figs. 2 and 3.

4.2. Effect of $|\mathbf{k}|^6$ Spectrum Imposition on the Wavy Crystalline Regime

One of the qualitatively distinct regimes that was isolated in our earlier two-dimensional collective coordinates study [6] was the “wavy crystalline” regime. This regime is distinguished by patterns consisting of particle columns that display a meandering displacement away from linearity. For $N = 418$, we have found the patterns to occur when $0.58 \leq \chi \leq 0.78$ [6]. An example of such a pattern is displayed in the top panel of Fig. 4. The result of applying the $|\mathbf{k}|^6$ spectrum minimization to this χ interval is our focus in this section. As above, we subjected randomly generated particle systems to the MINOP [24] algorithm to find the absolute minimum of the objective function Φ . Our \mathbf{k} -space parameter K is determined by the χ range over which the wavy crystalline regime prevails. While focusing on the $|\mathbf{k}|^6$ spectrum minimization problem, we have varied the independent coefficient D .

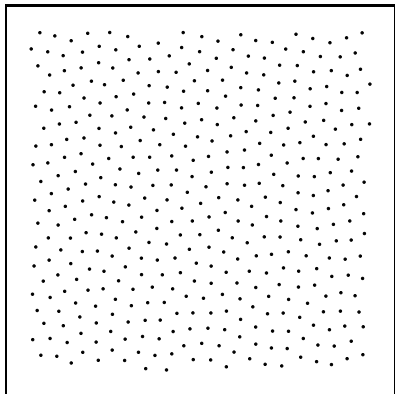
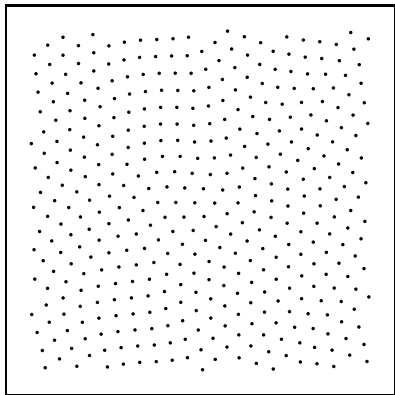
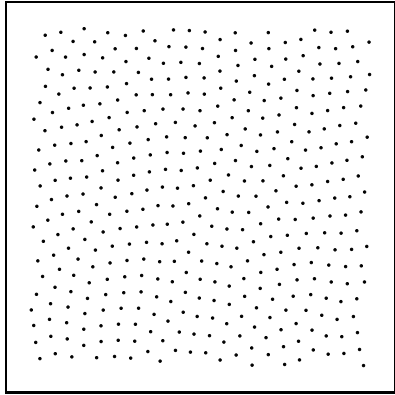


FIG. 4: Real space particle patterns for a system of 418 point particles. The $C(\mathbf{k})$ quantities for the wave vectors consistent with $\chi = 0.581339$ have been constrained. Top panel: Particle pattern in the wavy crystalline regime ($D = 0$). Middle panel: Particle pattern on which the $|\mathbf{k}|^6$ spectrum has been imposed with $DK^6 = 0.01$. Bottom panel: Particle pattern on which the $|\mathbf{k}|^6$ spectrum has been imposed with $DK^6 = 10$.

The middle and bottom panels of Fig. 4 display 418-particle configurations that result from imposing the $|\mathbf{k}|^6$ spectrum on particle systems that at $D = 0$ lie in the wavy crystalline regime. The multiplicative parameter D used in generating the configurations in the middle and bottom panels is low ($DK^6 = 0.01$) and high ($DK^6 = 10$), respectively, and the cutoff K is near the lower limit of the wavy regime of interest. It is important to note that all three particle patterns in Fig. 4 were formed from a common initial configuration. A comparison of the three figures reveals distortion and disruption of the meandering nature of the reference ($D = 0$) configuration that intensifies as D increases. Evidently the previously documented [6] tendency at $D = 0$ for increasing χ to herd particles towards a crystalline arrangement is sabotaged by allowing D to increase.

5. RESULTS - THREE DIMENSIONS

In this section, we discuss results for three-dimensional configurations that have been subjected to the computational algorithm, MINOP [24] requiring absolute minimization of Φ and $\tilde{\Phi}$. First, we extend our two-dimensional analysis to the tailoring of the structure factor of three-dimensional particle systems. Second, we return to an examination of the configurational patterns associated with constrained collective density variables in three dimensions. This latter aspect extends our earlier work in one [5] and two [6] dimensions. Note that all calculations presented in this section have been carried out to the same high precision as for the two-dimensional samples discussed in the preceding Sec. 4.

5.1. Tailoring the Structure Factor $S(k)$ - Three Dimensions

Our numerical calculations minimizing Φ have involved 256- and 500-particle systems. Note that these system sizes conform to the guideline discussed in Sec. 3. We vary the \mathbf{k} -space range parameter K ($2\pi \leq K \leq 40\pi$), the multiplicative parameter D ($0.01 \leq DK^\alpha \leq 180$), and investigate both the $\alpha = 1$ Harrison-Zeldovich spectrum and the $\alpha = 6$ minimization problem.

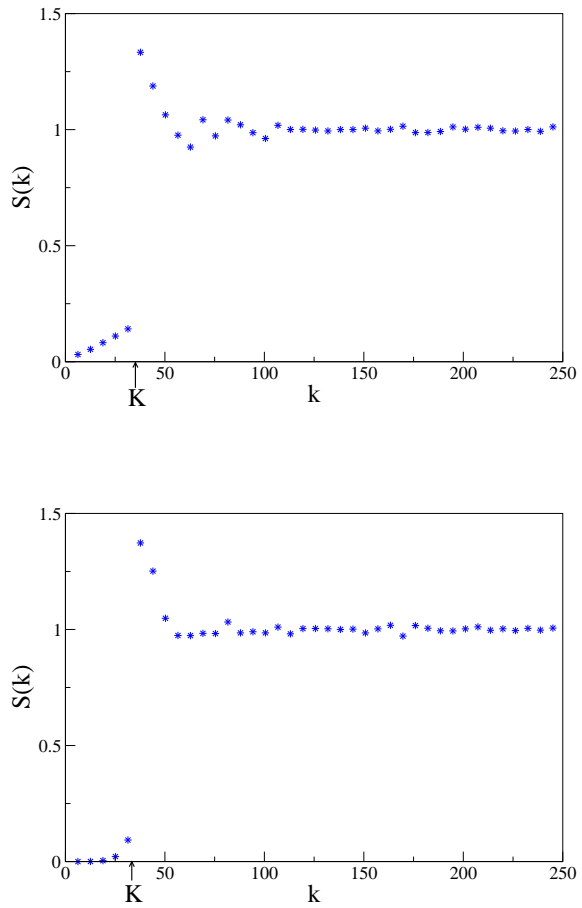


FIG. 5: (Color online) Averaged structure factor plots for the three-dimensional minimization problem. The relevant parameters are $N = 256$, $K = 10\pi$, $DK^\alpha = 20$, $\chi = 0.334635$. Top panel: Harrison-Zeldovich spectrum. Bottom panel: $|k|^6$ spectrum. Each structure factor is averaged over 6 realizations.

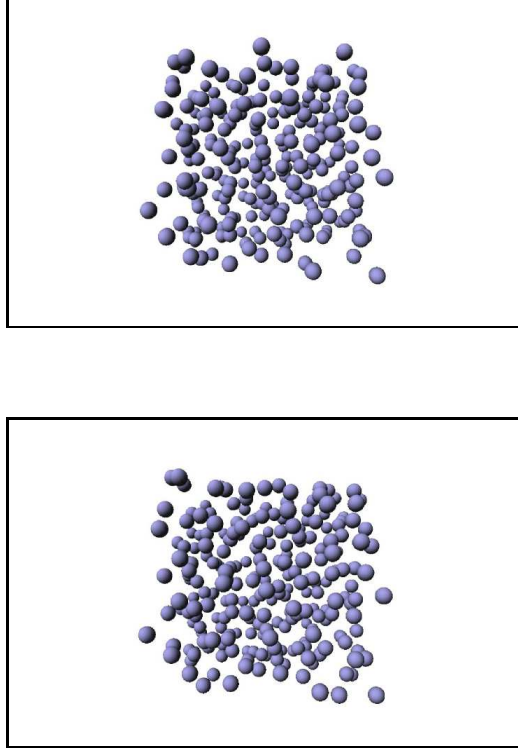


FIG. 6: (Color online) Snapshots of three-dimensional final configurations for investigated spectra. The relevant parameters are $N = 256$, $K = 10\pi$, $DK^\alpha = 20$, $\chi = 0.334635$. Top panel: Harrison-Zeldovich spectrum. Bottom panel: $|\mathbf{k}|^6$ spectrum.

As before, structure factors are derived from final configurations averaged over several realizations. The linear Harrison-Zeldovich and $|\mathbf{k}|^6$ cases are displayed in Fig. 5. Similarly to the two-dimensional study, the tailored structure factor deviates irregularly for $|\mathbf{k}| > K$ prior to averaging over a set of realizations. Once again the averaged $S(k)$ exhibits a peak just beyond $|\mathbf{k}| = K$, now an even stronger feature than in the two-dimensional cases shown earlier in Fig. 2. An examination of the plotted structure factors clearly reveals the linear and sextic nature of the two curves near the origin. Figure 6 displays representative three-dimensional final configurations for the Φ minimization problem for both the linear Harrison-Zeldovich and $|\mathbf{k}|^6$ spectra. The high degree of disorder is evident in both sample configurations.

A system-size scaling study was performed as part of our investigation. This is relevant to the approach to the thermodynamic limit. Specifically, we compared the simulation times for two different system sizes of fixed χ (appropriately scaled independent parameters N ,

K , and D) for the Harrison-Zeldovich spectrum. We find that doubling the system size increases the computation time by approximately a factor of 10.

5.2. Minimizing Collective Density Variables $C(\mathbf{k})$ - Three Dimensions

Our numerical studies for $D = 0$ concentrated on two system sizes ($N = 108$ and 500), a wide range of \mathbf{k} -space constraints *i.e.* low through high K , and a variety of initial configurations (both random and lattice-based). For the wide range of \mathbf{k} -space traversed, the odds of hitting relative minima of the total energy function $\tilde{\Phi}$ was increased for large K . However, trajectories converged to the absolute $\tilde{\Phi}$ minimum for all cases that were included in our final analysis. Our findings remain substantially consistent between the two investigated system sizes.

TABLE I: Classification of investigated cases associated with each of the regimes. Note that the multiplicative parameter $D = 0$ for this objective function $\tilde{\Phi}$ minimization problem.

N	Disordered Regime	Crystalline Regime
108	$\chi \leq 0.469136$	$\chi \geq 0.524691$
500	$\chi \leq 0.500666$	$\chi \geq 0.516666$

In the course of our investigation, we observed two distinct regimes of the final configurations as χ (see Eq. 4.1) was varied: disordered and crystalline. Table I presents the relevant range in χ for the two investigated systems and distinguishable regimes. The table indicates disorder for low values of χ and crystallinity for high values of χ . This is expected by analogy with the reported results of the one- [5] and two-dimensional [6] articles on collective density variables. However, our three-dimensional analysis indicates an abrupt transition from disordered to crystalline regimes revealing the lack of an intermediate “wavy crystalline” regime as observed in two dimensions. For the 500-particle system and $\chi \geq 0.516666$, we have verified that the crystal structure is a face-centered cubic lattice, which for the density of the system is consistent with the predictions of Sütő [7].

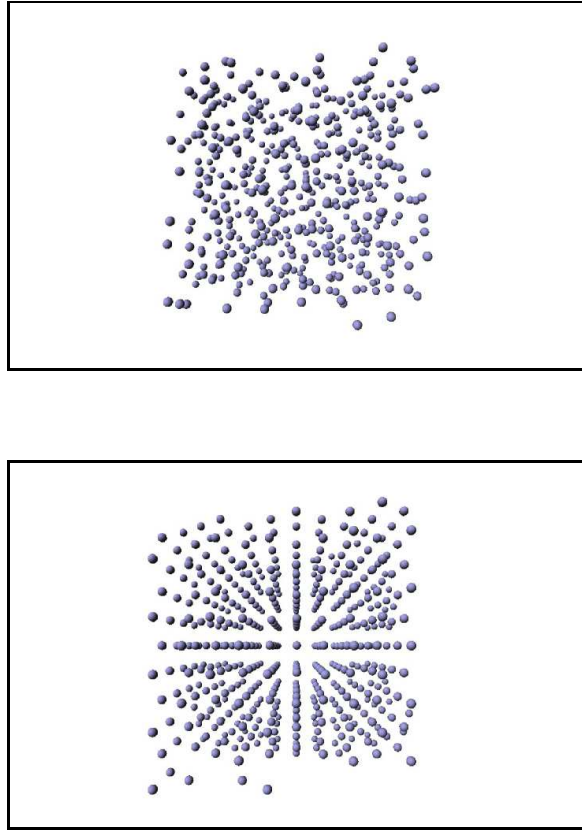


FIG. 7: (Color online) Real space particle patterns for the two distinct regimes for systems of 500 point particles. Top panel: Particle pattern in the disordered regime. The $C(\mathbf{k})$ quantities consistent with parameter $\chi = 0.171333$ have been constrained to their minimum values $-N/2$. Bottom panel: Particle pattern in the crystalline regime. The $C(\mathbf{k})$ quantities consistent with parameter $\chi = 0.702666$ have been constrained to their minimum values $-N/2$.

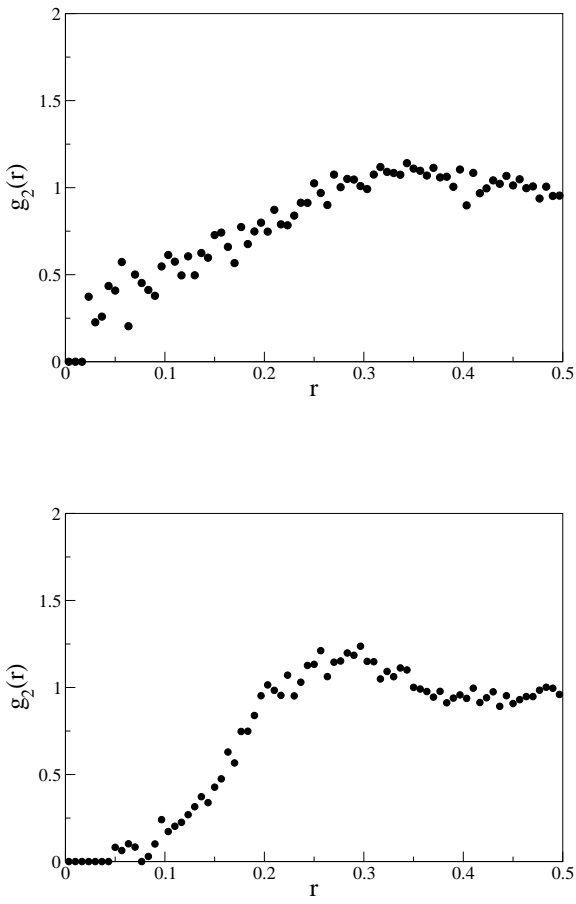


FIG. 8: Radial distribution functions for systems of 108 point particles. Top panel: The $C(\mathbf{k})$ quantities consistent with parameter $\chi = 0.123457$ have been constrained to their minimum values $-N/2$. Bottom panel: The $C(\mathbf{k})$ quantities consistent with parameter $\chi = 0.262346$ have been constrained to their minimum values $-N/2$. Each radial distribution function is averaged over 10 realizations.

Particle patterns respectively within the disordered (top panel) and crystalline (bottom panel) regimes for $N = 500$ are displayed in Fig. 7. The examples shown are typical for the two regimes and are vividly distinct. Further insight into the generated point patterns follows from examination of the associated pair correlation functions [18] (see Fig. 8). The emergence of an effective repulsive core for increasing values of χ is apparent, reminiscent of a similar effect observed in Ref. [6] in the two-dimensional case.

6. CONCLUSIONS AND DISCUSSION

The former studies of collective coordinate properties presented in Refs. [5] and [6] were restricted to one- and two-dimensional point patterns, and documented the effect of forcing sets of the collective variables for $|\mathbf{k}| \leq K$ to their individual absolute minima. The present investigation extends that analysis in two distinct directions, by considering point patterns in three dimensions, and by examining the effect of constraining the collective variables around the \mathbf{k} -space origin to chosen increments above their absolute minima. Specific assignments of the increments that have been considered have the form $D|\mathbf{k}|^\alpha$, where $D > 0$, and $\alpha = 1, 4, 6, 8$, and 10 . Point particle configurations satisfying these various collective variable constraints have been obtained to high numerical precision starting from both random and from distorted-crystal initial conditions, followed by minimization of appropriate objective functions [Φ and $\tilde{\Phi}$, Eqs. 2.4 and 2.10]. Although previous attempts have produced configurations for which the associated structure factor $S(k) \propto k^\alpha$ with $\alpha \leq 4$ [17, 28], our analysis also yields specific configurations that exhibit $S(k) \propto k^\alpha$ with $\alpha \geq 6$. In addition to the specific cases reported in this paper, our studies reveal that a considerably wider range of constrained $C(\mathbf{k})$ patterns can be imposed on many-particle systems. For example, forcing $C(\mathbf{k})$ to equal 0 instead of its absolute minimum $-N/2$, reveals a tendency to produce a high degree of disorder in the generated particle systems.

When $D = 0$, increasing the fraction χ of system degrees of freedom subject to collective variable constraints was found in one and two dimensions to drive the point particle configurations more and more toward crystalline periodicity. The present extension not surprisingly shows that the same qualitative trend applies to three dimensions as well. However the “wavy crystalline” regime reported in Ref. [6] to separate the two-dimensional low- χ disordered regime from the high- χ crystalline regime appears to have no three-dimensional analog. As χ increases for $D = 0$ cases in three dimensions, the relevant $\tilde{\Phi}$ landscape on which numerical absolute minimization needs to be carried out develops an increasing density of relative minima, thereby inhibiting (but not necessarily preventing) the search for qualifying particle configurations. For the few cases considered, increasing D above zero at constant χ has the effect of disrupting the tendency toward crystalline order.

A characteristic feature of the various cases examined, provided that the fraction χ is below its maximum value to yield valid solutions, is degeneracy of the final particle configurations. This is obvious when several independent initial configurations for a case considered are individually subjected to the same minimization operation, and then produce geometrically distinct final patterns. The minimized objective functions Φ and $\tilde{\Phi}$, for $D > 0$ and $D = 0$ cases respectively, indicate that these configuration sets are degenerate classical ground states, including disordered ones, for specific potential energy functions. When Φ is used, that potential function consists of four, three and two body components, while for $\tilde{\Phi}$ only two-body components arise. This offers a specific constructive method to achieve degenerate-ground-state potentials, a subject recently discussed by Sütő [7].

The present collective variable approach may also supply some insight into the existence of potentials whose classical ground states are amorphous, or at least highly irregular. Start with a small- χ constraint case, satisfied with an irregular point-particle configuration. This specific configuration will display specific $C(\mathbf{k})$ values for the unconstrained range $|\mathbf{k}| > K$. Next, formally expand the constraint radius K to the point where $\chi = 1$, regarding the already-obtained collective variable values as constraint targets. The irregular configuration in hand becomes automatically and trivially a proper solution for this extended problem. The resulting potential energy specified by Φ or $\tilde{\Phi}$ then possesses that irregular configuration as its unique classical ground state (aside from overall translations).

Acknowledgements

The authors thank Andrea Gabrielli and Michael Joyce for discussions concerning several aspects of the work reported in this paper. We gratefully acknowledge D. K. Stillinger for carrying out preliminary calculations that have provided useful guidelines for the work reported in this paper. S.T. and F.H.S. gratefully acknowledge the support of the Office of Basic Energy Sciences, DOE, under Grant No. DE-FG02-04ER46108. O.U.U. gratefully acknowledges the support of the Department of Energy CSGF fellowship.

[1] R.P. Feynman, *Statistical Mechanics*, (Benjamin, Reading, MA, 1972).

[2] D. Pines, Solid State Phys., **1**, 367 (1955).

- [3] J.K. Percus and G.J. Yevick, Phys. Rev., **110**, 1 (1958).
- [4] H.C. Andersen and D. Chandler, J. Chem. Phys., **53**, 547 (1970).
- [5] Y. Fan, J.K. Percus, D.K. Stillinger, and F.H. Stillinger, Phys. Rev. A, **44**, 2394 (1991).
- [6] O.U. Uche, F.H. Stillinger, and S. Torquato, Phys. Rev. E, **70**, 046122 (2004).
- [7] A. Sütő, Phys. Rev. Letters, **95**, 265501 (2005).
- [8] M.J. Mandell, J.P. McTague, and A. Rahman, J. Chem. Phys., **64**, 3699 (1976).
- [9] E. Leutheusser, Phys. Rev. A, **29**, 2765 (1983).
- [10] P.G. Debenedetti, *Metastable Liquids: Concepts and Principles*, (Princeton University Press, Princeton, NJ, 1996), pp. 282-301.
- [11] S. Torquato and F.H. Stillinger, Phys. Rev. E, **68**, 041113 (2003); publisher's note: Phys. Rev. E, **68**, 069901 (2003).
- [12] Hyperuniform systems have also been called superhomogeneous by Gabrielli, Joyce, and Labini, Phys. Rev. D, **65**, 083523 (2002).
- [13] R.P. Feynman, Phys. Rev., **94**, 262 (1954).
- [14] R.P. Feynman and M. Cohen, Phys. Rev., **102**, 1189 (1956).
- [15] L. Reatto and G.V. Chester, Phys. Rev., **155**, 88 (1967).
- [16] A. Donev, F.H. Stillinger, and S. Torquato, Phys. Rev. Lett., **95**, 090604 (2005).
- [17] A. Gabrielli, M. Joyce, and F.S. Labini, Phys. Rev. D, **65**, 083523 (2002).
- [18] S. Torquato, *Random Heterogeneous Materials: Microstructure and Macroscopic Properties*, (Springer-Verlag, New York, 2002).
- [19] S. Torquato and F. H. Stillinger, J. Phys. Chem. B, **106**, 8354 (2002); **106**, 11406 (2002).
- [20] J. Crawford, S. Torquato, and F. H. Stillinger, J. Chem. Phys., **119**, 7065 (2003).
- [21] O. U. Uche, F. H. Stillinger, and S. Torquato, Physica A, **360**, 21 (2006).
- [22] S. Torquato and F. H. Stillinger, Phys. Rev. E, **73**, 031106 (2006); S. Torquato and F. H. Stillinger, Experimental Math., in press.
- [23] O. Costin and J. Lebowitz, J. Phys. Chem. B, **108**, 19614, (2004).
- [24] J.E. Dennis and H.W Mei, J. Optim. Theory Appl., **28**, 455 (1979).
- [25] L. Kaufman, SIAM J. Optim., **10**, 56 (1999).
- [26] M. Abramowitz and I.A. Stegun, editors, *Handbook of Mathematical Functions*, (National Bureau of Standards Applied Mathematics Series No. 55, U.S. Government Printing Office, Washington, D.C., Ninth Printing, 1970).

- [27] W.H. Press, B.P. Flannery, S.A. Teukolsky, and W.T. Vetterling, *Numerical Recipes*, (Cambridge University Press, Cambridge, 1986).
- [28] A. Gabrielli, Phys. Rev. E, **70**, 066131 (2004).